Int. J. Electrochem. Sci., 9 **(2014)** 6529 - 6550

International Journal of
ELECTROCHEMICAL
SCIENCE
www.electrochemsci.org

Corrosion Inhibitive Effect of Synthesized Thiourea Derivatives on Mild Steel in a 15% HCl Solution

Mahendra Yadav[1,*], *Sushil Kumar*[1], *Indra Bahadur*[2], *Deresh Ramjugernath*[2,*]

[1]Department of Applied Chemistry, Indian School of Mines, Dhanbad, 826004, India
[2]Thermodynamics Research Unit, School of Engineering, University of KwaZulu-Natal, Howard College Campus, King George V Avenue, Durban, 4041, South Africa
[*]E-mail: yadav_drmahendra@yahoo.co.in; ramjuger@ukzn.ac.za

Received: 9 June 2014 / *Accepted:* 7 August 2014 / *Published:* 25 August 2014

In this study, the inhibitive performance of two synthesized thiourea derivatives, namely, 1-(3-mercapto-5-(pyridin-4-yl)-4H-1,2,4-triazol-4-yl)-3-phenylthiourea (MPTP), 1-(3-mercapto-5-(pyridin-4-yl)-4H-1,2,4-triazol-4-yl)-3-(4-methoxyphenyl) thiourea (MPTMP) were studied for mild steel corrosion in a 15% HCl solution using weight loss measurements, potentiodynamic polarization, and electrochemical impedance spectroscopy (EIS) techniques. The inhibition efficiency of both the inhibitors increased with an increase in the concentration of inhibitor. The inhibitors MPTP and MPTMP show a corrosion inhibition efficiency of 94.3% and 96.8% respectively, in 50 ppm concentrations at 303 K. Polarization studies showed that both inhibitors studied were of a mixed type in nature. The adsorption of inhibitors on the mild steel surface obey the Langmuir adsorption isotherm. Scanning electron microscopy (SEM), energy dispersive X-ray spectroscopy (EDX), UV-Visible spectroscopy, and atomic force microscopy (AFM) were performed for a surface study of uninhibited and inhibited mild steel samples. The semi-empirical AM1 method was employed for theoretical calculations.

Keywords: Mild steel; Thiourea derivatives; EIS; Polarization; Corrosion inhibition; Quantum study

1. INTRODUCTION

Corrosion of mild steel occurs widely in various industrial fields and results in huge economic losses and possesses many potential safety problems [1–3]. Among the numerous anticorrosion measures, corrosion inhibition is widely used and acts as one of the most economical and effective ways [4–7] to mitigate against corrosion. The study of corrosion processes and their inhibition by organic inhibitors is a very active field of research [5]. Many researchers have reported that the inhibition effect depends mainly on some physico-chemical and electronic properties of the organic

inhibitor which is related to its functional groups, steric effects, electronic density of donor atoms, and orbital character of donating electrons, etc. [6,7]. The inhibiting mechanism is generally explained by the formation of a physically and/or chemically adsorbed film on the metal surface [8, 9]. It is well known that organic compounds which act as inhibitors are rich in heteroatoms, such as sulphur, nitrogen, and oxygen [10, 11]. Some substituted thiourea derivatives have been studied in considerable detail as effective corrosion inhibitors for mild steel in acidic media [12-18].

In a continuation of our research for developing corrosion inhibitors [19-21] with high effectiveness and efficiency, the present investigation explores a systematic study to ascertain the inhibitive action of synthesized thiourea derivatives, namely, 1-(3-mercapto-5-(pyridin-4-yl)-4H-1,2,4-triazol-4-yl)-3-phenylthiourea (MPTP), 1-(3-mercapto-5-(pyridin-4-yl)-4H-1,2,4-triazol-4-yl)-3-(4-methoxyphenyl) thiourea (MPTMP) on corrosion of mild steel in a 15% HCl solution by using weight loss measurement, potentiodynamic polarization, AC impedance and quantum chemical calculations.

2. EXPERIMENTAL PROCEDURES

2.1. Synthesis of inhibitors

The inhibitors were synthesized by the method reported in literature [22]. The synthesis route for the inhibitors (MPTP and MPTMP) is shown in Scheme 1 and the structure of the inhibitors is shown in Figure 1. The purity of the inhibitors was checked by thin layer chromatography (TLC). The melting point, yield, and IR data of the synthesized compounds are given below:

MPTP

Yield (77%), m.p. = 112-114 °C.

IR (ν/cm^{-1}): 3240 (NH), 1665 (C=N), 1350 (C=S), 2560 (SH)

MPTMP

Yield (79%), m.p. = 118-120 °C.

IR (ν/cm^{-1}): 3260 (NH), 1660 (C=N), 1360 (C=S), 2550 (SH), 2940 (CH alkyl)

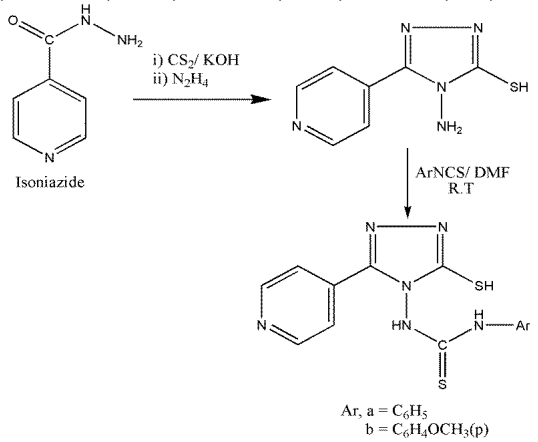

Scheme 1. Synthesis route for the inhibitors 1-(3-mercapto-5-(pyridin-4-yl)-4H-1,2,4-triazol-4-yl)-3-phenylthiourea (MPTP) and 1-(3-mercapto-5-(pyridin-4-yl)-4H-1,2,4-triazol-4-yl)-3-(4-methoxyphenyl) thiourea (MPTMP).

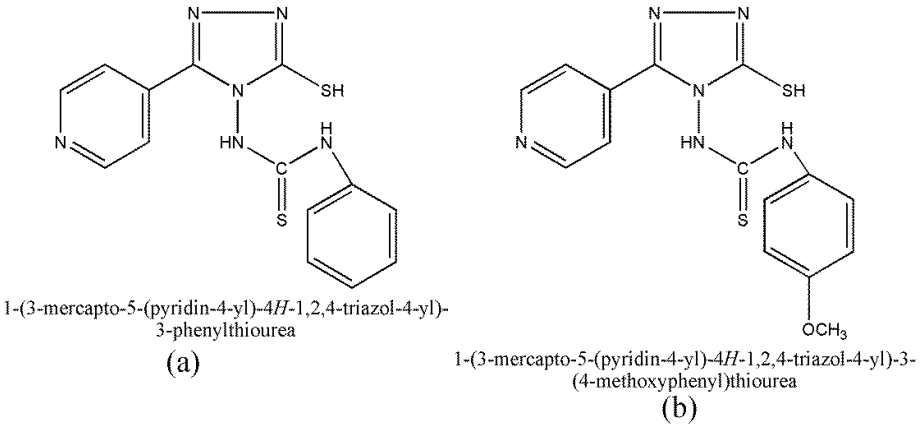

Figure 1. Structure of the inhibitors 1-(3-mercapto-5-(pyridin-4-yl)-4H-1,2,4-triazol-4-yl)-3-phenylthiourea (MPTP) and 1-(3-mercapto-5-(pyridin-4-yl)-4H-1,2,4-triazol-4-yl)-3-(4-methoxyphenyl) thiourea (MPTMP).

2.2. Mild steel sample

Weight loss and electrochemical studies were performed on a freshly prepared sheet of mild steel having a composition (wt.%): C, 0.12; Mn, 0.11; Cu, 0.01; Si, 0.02; Sn, 0.01; P, 0.02; Ni, 0.02 and the remaining fraction Fe. Mild steel samples used in the weight loss experiment were mechanically cut into 3.0 cm × 3.0 cm × 0.1 cm dimensions, and abraded with SiC abrasive papers of grade 320, 400 and 600. For potentiodynamic polarization and AC impedance studies, mild steel samples having dimension 1.0 cm × 1.0 cm × 0.1 cm were mechanically cut and abraded similarly to the previous procedure, with an exposed area of 1 cm^2 (the remaining surface was covered with araldite resin) with a 3 cm long stem. Before starting the experiments, the mild steel samples were washed with distilled water, degreased in acetone, dried and stored in a vacuum desiccator.

2.3. Test solution

The test solutions (15% HCl solution) were prepared by dilution of analytical grade 37% HCl with distilled water. The concentration range of inhibitors was 10–50 ppm (mg L^{-1}) and the volume of test solution used for weight loss measurement and electrochemical studies was 250 mL and 150 mL, respectively.

2.4. Methods

2.4.1. Weight loss measurements

Gravimetric experiments were performed according to the standard methods [23]. The corrosion rate (*CR*), inhibition efficiency (η%) and surface coverage (θ) were determined by the following equations:

$$CR\left(\text{mmy}^{-1}\right)=\frac{8.76\times10^{4}\times W}{D\times A\times t} \quad (1)$$

where, W = weight loss (g), A = area of specimen (cm^2) exposed in solution, t = exposure time (h), and D = density of mild steel (g cm^{-3}).

$$\theta=\frac{CR_0-CR_i}{CR_0} \quad (2)$$

$$\eta(\%)=\frac{CR_0-CR_i}{CR_0}\times100 \quad (3)$$

where, CR_0 and CR_i are corrosion rates in the absence and presence of inhibitors.

2.4.2. Electrochemical Measurements

The electrochemical studies were conducted in a conventional three-electrode cell consisting of a mild steel sample of 1 cm^2 exposed area as the working electrode, a platinum counter electrode and a saturated calomel electrode (SCE) as the reference electrode, using CH electrochemical workstation (Model No: CHI 760D, manufactured by CH Instruments, Austin, USA) at 303 K. Before impedance or polarization measurements, the working electrode was immersed in the test solution until a steady-state of the open-circuit potential corresponding to the corrosion potential (E_{corr}) of the working electrode was obtained. Potentiodynamic polarization curves were obtained by changing the electrode potential from -200 to +200 mV vs. SCE at OCP at a scan rate of 1 mVs^{-1}. The linear Tafel segments of the anodic and cathodic curves were extrapolated to obtain corrosion current densities (i_{corr}).

Impedance measurements were carried out using AC signals of amplitude 10 mV peak to peak at the open circuit potential in the frequency range100 kHz to 10 mHz. All impedance data were fitted to appropriate circuits using ZSimpWin.3.21 software.

2.4.3. UV-visible spectra

The UV-visible absorption spectra of solutions containing optimum concentration (50 ppm) of inhibitor before and after immersion of the mild steel sample for 6 h were recorded using the Shimadzu model UV-160A spectrophotometer.

2.4.4. Scanning electron microscopic and energy dispersive spectroscopy analysis

For the surface morphological study of the uninhibited and inhibited mild steel samples, SEM and EDS images were recorded using the instrument HITACHI S3400N.

2.4.5. Atomic Force Microscopy

The AFM images of polished, uninhibited and inhibited mild steel samples were carried out using a Nanosurf Easyscan2 instrument, Model: NT-MDT, Russia; Solver Pro-47.

2.4.6. Quantum chemical study

Complete geometrical optimizations of the investigated molecules are performed using the semi-empirical AM1 method [24]. Theoretical parameters such as the energies of the highest occupied and lowest unoccupied molecular orbital (E_{HOMO} and E_{LUMO}), energy gap (ΔE) and dipole moment (μ) were determined.

3. RESULTS AND DISCUSSION

3.1. Weight loss measurements

3.1.1. Effect of inhibitor concentration and temperature

The values of corrosion rate (*CR*), surface coverage (θ) and corrosion inhibition efficiency (η%) obtained from weight loss measurements for the mild steel specimens immersed in 15% HCl solution in the absence and presence of different concentrations (10- 50 ppm) of inhibitors (MPTP, MPTMP) for an immersion period of 6 h at different temperatures (303-333 K) are listed in Table 1. From Table 1, it is apparent that the inhibition efficiency increased with an increasing concentration of the inhibitors. By increasing the inhibitor concentration, the part of metal surface covered by inhibitor molecules increases and this leads to an increase in the inhibition efficiencies [25].

Table 1. Corrosion parameters namely corrosion rate (*CR*), surface coverage (θ) and inhibition efficiency (η%) of mild steel in 15% HCl solution in the presence and absence of inhibitor at different temperatures, obtained from weight loss measurements.

	303 K			313 K			323 K			333 K		
Conc. (ppm)	*CR* (mmy^{-1})	θ	η %	*CR* (mmy^{-1})	θ	η %	*CR* (mmy^{-1})	θ	η %	*CR* (mmy^{-1})	θ	η %
Blank	28.2	-	-	58.1	-	-	98.9	-	-	144.5	-	-
MPTP												
10	5.35	0.81	81.0	12.31	0.78	78.8	22.35	0.77	77.4	35.98	0.75	75.1
20	3.60	0.87	87.2	8.65	0.85	85.1	15.62	0.84	84.2	26.44	0.81	81.7
30	2.59	0.90	90.8	6.27	0.89	89.2	11.77	0.88	88.1	20.95	0.85	85.5
50	1.60	0.94	94.3	4.30	0.92	92.6	8.20	0.91	91.7	15.60	0.89	89.2
MPTMP												
10	3.95	0.86	86.0	9.58	0.83	83.5	17.60	0.82	82.2	28.6	0.80	80.2
20	2.25	0.92	92.0	5.69	0.90	90.2	11.37	0.88	88.5	19.65	0.86	86.4
30	1.63	0.94	94.2	4.41	0.92	92.4	8.90	0.91	91.0	16.03	0.88	88.9
50	0.90	0.96	96.8	3.19	0.94	94.5	6.52	0.93	93.4	11.84	0.91	91.8

It is further evident from Table 1 that both the inhibitors have good inhibition even at concentrations, as low as 10 ppm. The inhibition efficiency of MPTMP and MPTP at a 50 ppm concentration was found to be 96.8% and 94.3% respectively, while it was 86.0% and 81.0% respectively, at a 10 ppm concentration at 303 K (Table1). The inhibition efficiency of both the inhibitors decreased with an increase in temperature from 303 to 333 K. This is due to the fact that at higher temperatures the metal dissolution process is enhanced and the adsorbed inhibitor molecules are partially desorbed from the metal surface [26].

3.1.2. Thermodynamic and activation parameters

To evaluate the adsorption and thermodynamic activation parameters of corrosion processes of mild steel in a 15% HCl solution, weight loss measurements were carried out in the temperature range 303–333 K in the absence and presence of inhibitors after 6 h of immersion. The apparent activation energy (E_a) for dissolution of mild steel in 15% HCl solution was calculated by using the Arrhenius equation:

$$\log CR = \frac{-E_a}{2.303RT} + \log A \qquad (4)$$

where R is the Universal gas constant (8.314 J $K^{-1}mol^{-1}$), T is the absolute temperature (K) and A is the Arrhenius pre-exponential factor. Figure 1 presents the Arrhenius plot of log CR against $1/T$ for the corrosion of mild steel in a 15% HCl solution in the absence and presence of inhibitors at concentrations ranging from 10 to 50 ppm. From Figure 2, the slope of individual line was determined, and the activation energy was calculated using the expression E_a = - slope × 2.303R. The calculated values of E_a are summarized in Table 2. It is evident from Table 2 that the values of the apparent activation energy for the inhibited solutions were higher than that for the uninhibited solution, indicating that the dissolution of mild steel was decreased due to formation of a barrier by the adsorption of the inhibitor on the metal surface [27]. The higher values of apparent activation energy (E_a) in the presence of inhibitor as compared to the E_a in the absence of inhibitor in 15% HCl solution indicates that the inhibitor induces the energy barrier for the corrosion reaction which leads to the decreasing of the rate of corrosion of mild steel in the presence of inhibitor. Furthermore, an increase in E_a with an increase in concentration of inhibitor (Table 2) suggested an increase in the energy barrier and a decrease in corrosion rate of mild steel.

The values of the standard enthalpy of activation (ΔH^*) and standard entropy of activation (ΔS^*) were calculated by using the transition state equation

$$CR = \frac{RT}{Nh}\exp\left(\frac{\Delta S^*}{R}\right)\exp\left(-\frac{\Delta H^*}{RT}\right) \qquad (5)$$

where, h is Planck's constant and N is the Avogadro number, respectively.

A plot of log (CR/T) against $1/T$ (Figure 3) gave straight lines with a slope of $-\Delta H^*/2.303R$ and an intercept of [log(R/Nh) + ($\Delta S^*/2.303R$)], from which the activation thermodynamic parameters (ΔH^* and ΔS^*) were calculated, as listed in Table 2. The positive sign of enthalpy reflects the endothermic nature of the mild steel dissolution process. The negative value of ΔS^* for both inhibitors indicates that the formation of the activated complex in the rate determining step represents an

association rather than a dissociation step, meaning that a decrease in disorder takes place during the course of the transition from reactants to activated complex [28].

Table 2. Activation parameter for mild steel in a 15% HCl solution in the absence and presence of inhibitor obtained from weight loss measurements

Inhibitor	Concentration (ppm)	E_a (kJmol^{-1})	ΔH^* (kJ mol^{-1})	ΔS^* (Jmol^{-1}K^{-1})
Blank	-	45.7	43.0	-74.5
MPTP	10	53.1	50.3	-63.9
	20	55.3	52.6	-60.0
	30	57.9	55.3	-54.0
	50	61.8	60.3	-41.3
MPTMP	10	55.0	60.8	-69.1
	20	60.5	68.5	-78.4
	30	63.5	43.0	-74.4
	50	71.0	52.4	-59.7

3.1.3. Adsorption isotherm

Information on the interaction between the inhibitor molecules and the mild steel surface can be provided by the adsorption isotherm. The surface coverage degrees (θ) calculated from weight loss measurements and corresponding to different concentrations of both the inhibitors in the 303–333 K temperature range, were used to study the adsorption behaviour of inhibitors and to choose the more suitable adsorption isotherm. Attempts were made to fit these values to various isotherms. The correlation coefficient and slope values were used to choose the isotherm that best fits the experimental data. The plots of C_{inh}/θ vs. C_{inh} yielded straight lines [Fig. 4] with the correlation coefficient (R^2) and slope values given in Table 3 at different temperatures. The correlation coefficient and slope values in Table 3 are close to unity indicating that the adsorption of both the inhibitors obey the Langmuir adsorption isotherm represented by the following equation:

$$\frac{C_{inh}}{\theta} = \frac{1}{K_{ads}} + C_{inh} \quad (6)$$

where C_{inh} is the inhibitor concentration, K_{ads} is the equilibrium constant for adsorption-desorption process.

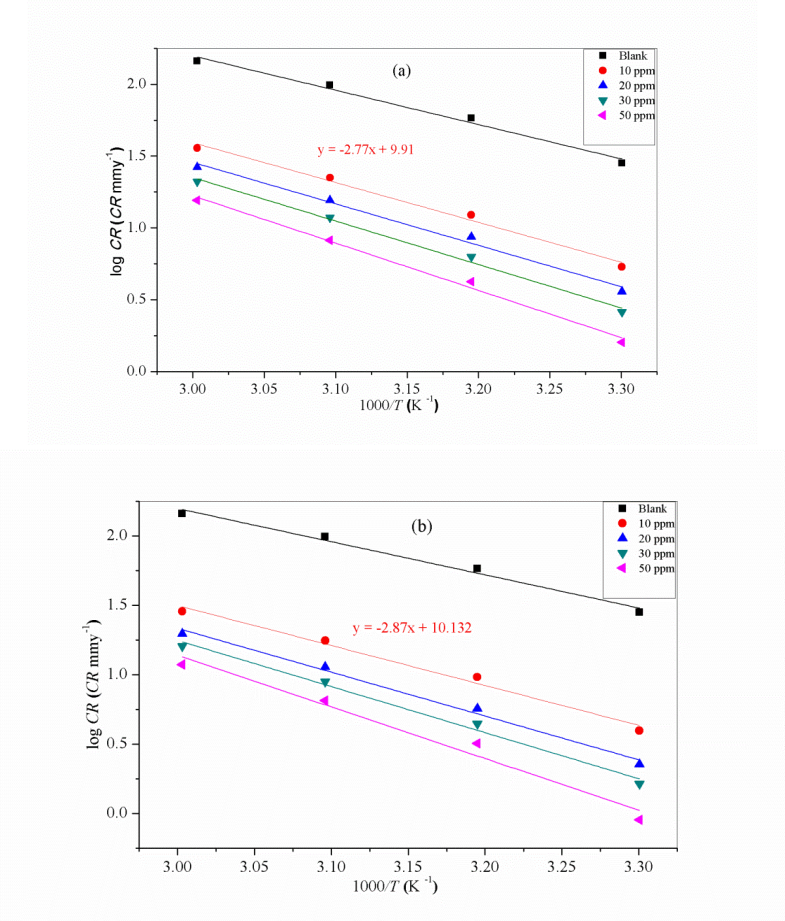

Figure 2. Arrhenius plots of log *CR* versus 1000/*T* for mild steel corrosion in a 15% HCl solution (a) MPTP (b) MPTMP.

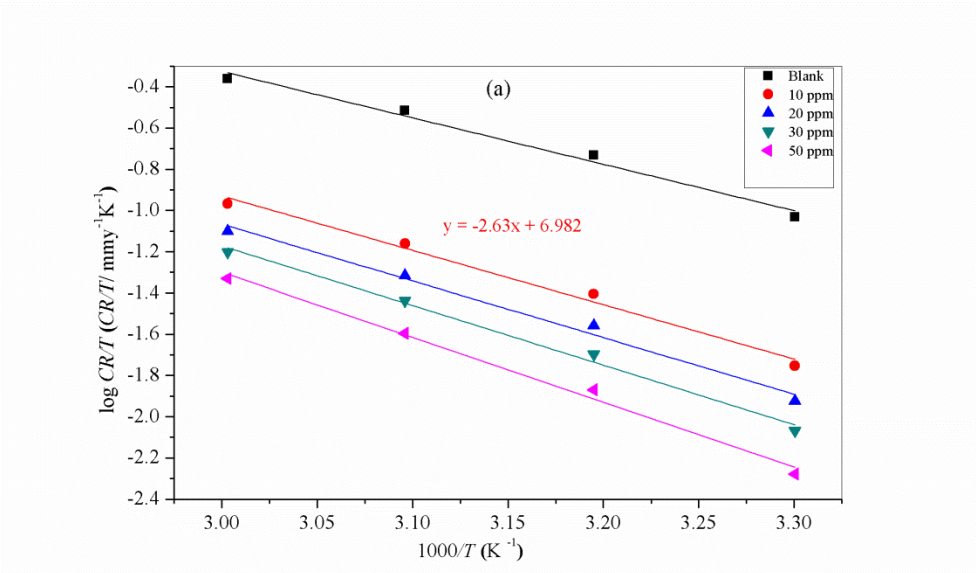

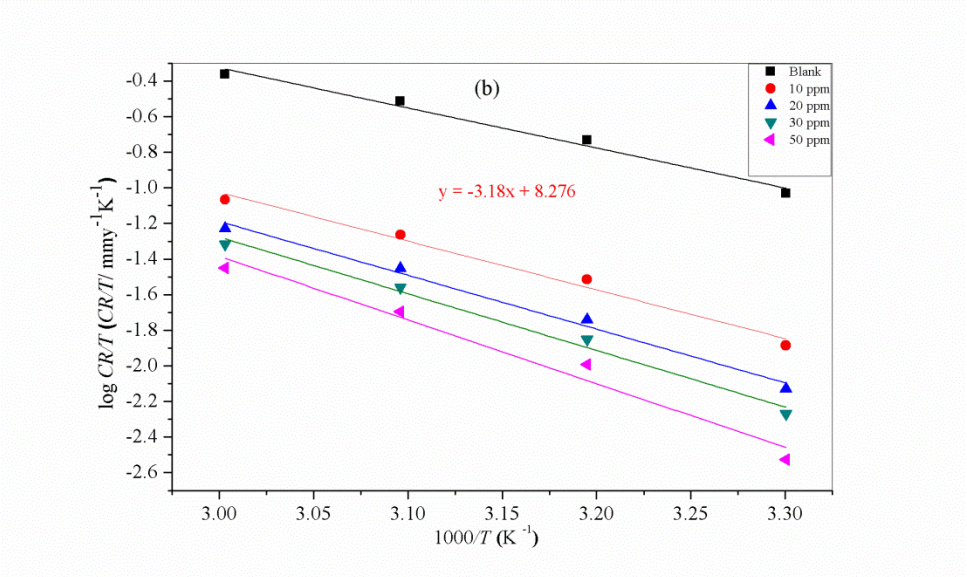

Figure 3. Transition state plot of log *CR* /*T* versus 1000/*T* for mild steel in a 15% HCl solution at different concentrations (a) MPTP (b) MPTMP.

Table 3. Adsorption parameters for MPTP and MPTMP calculated from Langmuir adsorption isotherm for mild steel in a 15% HCl solution in a temperature range of 303-333K

Inhibitor	Temperature (K)	K_{ads} (M^{-1})	ΔG°_{ads} (kJ mol^{-1})	Correlation coefficient (R^2)	Slope values
MPTP	303	1.27×10^5	-38.7	0.998	1.01
	313	1.18×10^5	-37.8	0.997	1.03
	323	1.15×10^5	-35.4	0.995	1.04
	333	1.02×10^5	-34.2	0.992	1.06
MPTMP	303	2.02×10^5	-39.8	0.999	1.00
	313	1.80×10^5	-38.9	0.998	1.02
	323	1.65×10^5	-37.4	0.996	1.03
	333	1.53×10^5	-36.1	0.994	1.05

The values of K_{ads} were calculated from the intercept of Figure 4. Large values of K_{ads} obtained for both inhibitors studied suggest more efficient adsorption and hence better corrosion inhibition efficiency. Using the values of K_{ads} , the values of ΔG°_{ads} were obtained by using the following equation:

$$\Delta G^{0}_{ads} = -RT\ln\left(55.5K_{ads}\right) \quad (7)$$

The value of 55.5 is the concentration of water in solution in mol L^{-1}. Calculated values of K_{ads} and ΔG°_{ads} are listed in Table 3. The negative values of ΔG°_{ads} indicate spontaneous adsorption of inhibitor molecules onto the mild steel surface and strong interactions between inhibitor molecules and the metal surface. It is also seen that the values of ΔG°_{ads} increased with an increase in inhibitor concentration, a phenomenon which indicates that the adsorption of the inhibitor onto the mild steel surface was favorable with increasing inhibitor concentrations. In general, values of ΔG°_{ads} up to −20

kJmol^{-1} are compatible with physisorption and those which are more negative than −40 kJmol^{-1} involve chemisorptions [29]. The calculated ΔG°_{ads} values for MPTP and MPTMP were found in the range of -38.7 to –34.2 and -39.8 to –36.1 kJmol^{-1}, respectively, at different temperatures (303-333 K); these values were between the threshold values for physical adsorption and chemical adsorption, indicating that the adsorption process of inhibitors on the mild steel surface involve both the physical as well as chemical adsorption.

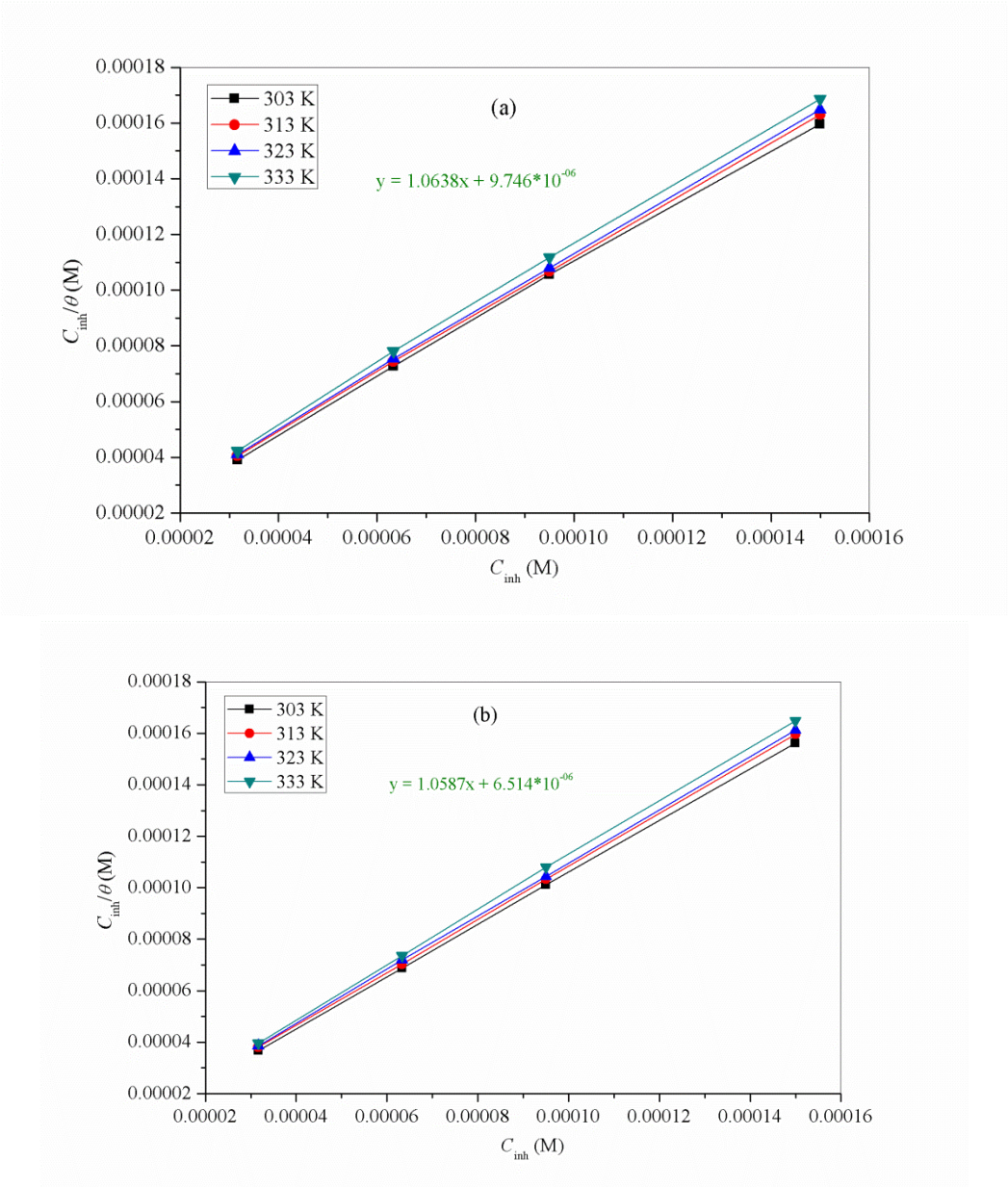

Figure 4. Langmuir plots of (C_{inh}/θ) versus C_{inh} for (a) MPTP (b) MPTMP.

3.2. Electrochemical studies

3.2.1. Polarization studies

The potentiodynamic polarization curves for mild steel in a 15% HCl solution in the absence and presence of different concentrations of MPTP and MPTMP are shown in Figure 5 (a, b) at 303 K. The corrosion parameters such as corrosion potential (E_{corr}), anodic Tafel slope (β_a), cathodic Tafel slope (β_c) and corrosion current density (i_{corr}) obtained from these curves are given in Table 4. The percentage inhibition efficiency (η%) was calculated using the equation

$$\eta(\%) = \frac{i^0_{corr} - i_{corr}}{i^0_{corr}} \times 100 \qquad (8)$$

where, i^0_{corr} and i_{corr} are the values of the corrosion current density in the absence and presence of inhibitors, respectively.

Table 4. Electrochemical parameter and percentage inhibition efficiency (η *%)* obtained from polarisation studies for mild steel in a 15% HCl solution in the absence and presence of inhibitor at 303 K.

Inhibitor	Conc (ppm)	$-E_{corr}$ (mV/SCE)	i_{corr} (μA cm^{-2})	β_a (mVdec^{-1})	β_c (mV dec^{-1})	η(%)
Blank	-	416	6733	332	338	-
MPTP	10	455	1191	299	277	82.3
	20	431	737	221	274	88.7
	30	438	499	290	296	92.5
	50	447	342	375	269	94.9
MPTMP	10	460	782	283	270	88.4
	20	437	396	437	279	94.1
	30	422	325	482	279	95.1
	50	452	109	532	306	98.3

It is apparent from Fig.5, that both anodic metal dissolution of iron and cathodic hydrogen evolution reaction were inhibited after the addition of inhibitors to a 15% HCl solution. The inhibition of these reactions was more pronounced on increasing the inhibitors concentration. The lower corrosion current density (i_{corr}) values in the presence of inhibitor suggest that the inhibitor molecules adsorbed on the surface of mild steel, thereby blocking the corrosion reaction [30] and increasing the inhibition efficiency. The efficiency of the inhibitors followed the order: MPTMP > MPTP at 303 K. The anodic Tafel slope (β_a) and the cathodic Tafel slope (β_c) of MPTP and MPTMP changed with inhibitor concentration, indicating that these inhibitors controlled both anodic as well as cathodic reactions and act as mixed inhibitors.

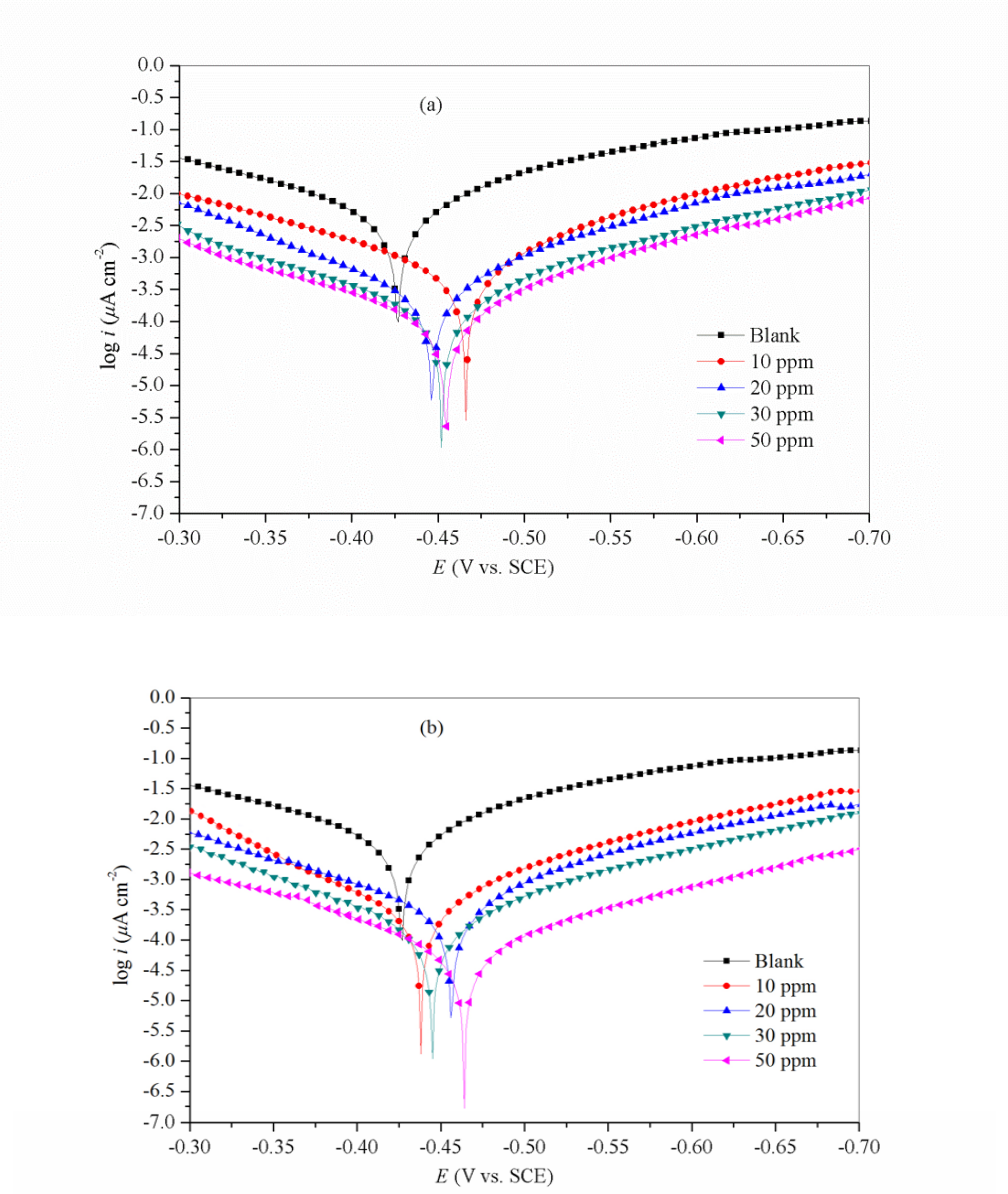

Figure 5. Potentiodynamic polarization curves for mild steel in a 15% HCl solution in the presence and absence of inhibitor 303 K (a) MPTP (b) MPTMP.

The presence of inhibitor causes minor change in E_{corr} values with respect to the E_{corr} value in the absence of inhibitor. If the change in E_{corr} value in the presence of inhibitor with respect to the E_{corr} value in the absence of inhibitor is more than 85 mV, the inhibitor is recognized as an anodic or a cathodic type inhibitor whereas if the change in E_{corr} value is less than 85 mV, the inhibitor is recognized as a mixed type inhibitor [31]. In the present investigation the maximum shift in E_{corr} was 44 mV towards the cathodic direction indicating that the inhibitors MPTP and MPTMP act as mixed type inhibitors with a predominately cathodic effect.

3.2.2. EIS studies

Adsorption of a protective inhibitor on the metal surface causes a significant increase in impedance of the corrosion system, thus causing an increase in the resistance to the charge transfer process. Therefore, the performance of an inhibitor can be determined by impedance measurements of the corrosion system. The degree of the corrosion protection can be determined by comparing the impedance obtained in the presence and absence of inhibitors in the corrosive environment. The Nyquist plots for mild steel obtained at mild steel / 15% HCl solution interface with and without the different concentrations of MPTP and MPTMP at 303 K are shown in Figure 6. The existence of a depressed semicircle with its center below the axis ($Z^{'}$) in the Nyquist plots (Fig.6 a, b) for both inhibitors suggest the non-homogeneity and roughness of the mild steel surface [32]. The EIS spectra of all tests were analyzed using the equivalent circuit shown in Figure 7, which is a parallel combination of the charge transfer resistance (R_{ct}) and the constant phase element (CPE), both in series with the solution resistance (R_s). This type of electrochemical equivalent circuit was reported previously to model the iron/acid interface [33]. A constant phase element (CPE) is introduced instead of a pure double layer capacitance to give a more accurate fit as the double layer at interface does not behave as an ideal capacitor.

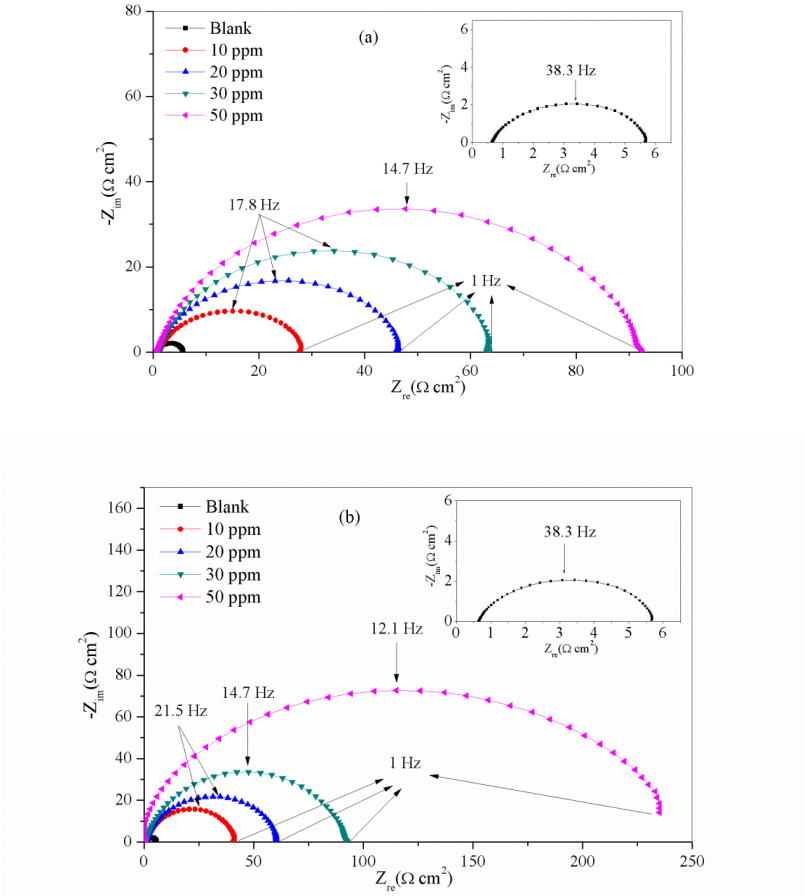

Figure 6. Nyquist plots for mild steel in a 15% HCl solution (a) MPTP (b) MPTMP containing various concentrations (1) 0 ppm (2) 10 ppm (3) 20 ppm (4) 30 ppm (5) 50 ppm at 303 K.

The electrochemical parameters such as solution resistance, charge transfer resistance and CPE constants (Y0 and n) obtained from the fitting of the experimental data of Nyquist plots in the equivalent circuit shown in Fig. 7 are presented in Table 5.

The inhibition efficiency (η%) was calculated from charge transfer resistance values obtained from impedance measurements using the following relation

$$\eta(\%) = \frac{R_{ct\,(inh)} - R_{ct}}{R_{ct\,(inh)}} \times 100 \qquad (9)$$

where $R_{ct(inh)}$ and R_{ct} are the charge transfer resistances in presence and absence of inhibitor respectively.

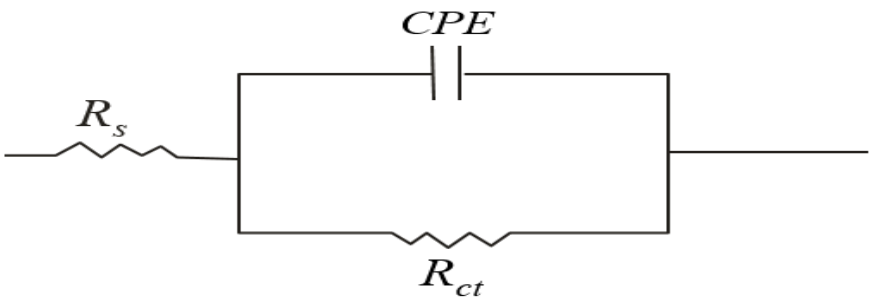

Figure 7. Equivalent circuit diagram

Table 5. Electrochemical impedance parameters for mild steel in a 15% HCl solution in the absence and presence of inhibitor at different concentration at 303 K

	Conc.(ppm)	R_s (Ω cm^2)	R_{ct} (Ω cm^2)	Y_o(μF cm^{-2})	n	C_{dl} (μF cm^{-2})	η%
Blank	-	0.65	5.1	1471	0.87	721.1	-
MPTP	10	1.13	28.4	820	0.80	313.1	82.0
	20	0.83	45.2	344	0.85	167.3	88.7
	30	0.95	63.0	290	0.84	136.9	91.9
	50	0.30	108.8	200	0.87	114.6	95.3
MPTMP	10	0.90	40.4	394	0.84	184.4	87.4
	20	1.02	67.8	228	0.84	106.3	92.5
	30	0.76	89.8	180	0.85	87.0	94.3
	50	0.75	186.5	40	0.98	37.9	97.3

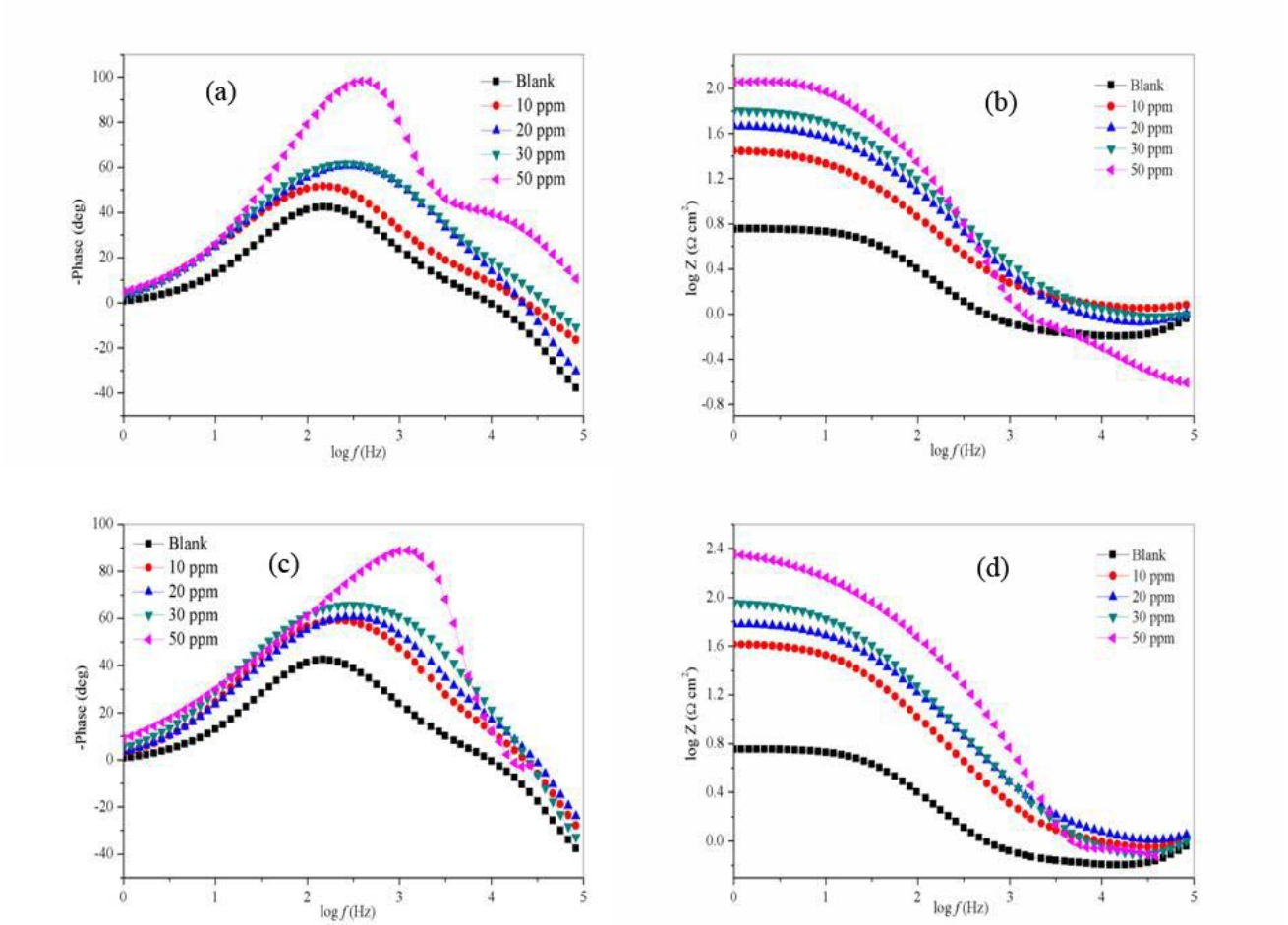

Figure 8. Bode plots for mild steel in a 15% HCl solution in the absence and presence of different concentrations of inhibitors (a) MPTP (b) MPTMP.

The values of the double layer capacitance (C_{dl}) were calculated from the charge transfer resistance and CPE parameters (Y_0 and n) using the expression [34]

$$C_{dl} = (Y_0 R_{ct}^{1-n})^{1/n} \quad (10)$$

where Y_0 is the CPE constant and n is the CPE exponent . The value of n represents the deviation from the ideal behavior and it lies between 0 and 1.

The data shown in Table 5 reveal that the value of R_{ct} increases with the addition of inhibitors as compared to the blank solution; the increase in R_{ct} value is attributed to the formation of a protective film at the metal/solution interface. The C_{dl} value decreases on increasing the concentration of both the inhibitors, indicating a decrease in the local dielectric constant and/or an increase in the thickness of the electrical double layer, suggesting that the inhibitor molecules are adsorbed at the metal/solution interface.

The Bode phase angle plots (Fig. 8 a, c) show a single maximum (one time constant) at intermediate frequencies, broadening of this maximum in the presence of inhibitors accounts for the formation of a protective layer on the electrode surface. Moreover, there is only one phase maximum in the Bode plot (Fig.8 a, c) for both inhibitors, indicating only one relaxation process, which would be the charge transfer process, taking place at the metal- electrolyte interface.

Figure 8 (b, d) shows that the impedance value in the presence of both inhibitors is larger than in the absence of inhibitors and the value of impedance increases on increasing the concentration of both inhibitors studied. This means that the corrosion rate is reduced in the presence of the inhibitors and continues to decrease with an increase in the concentration of inhibitors.

Electrochemical results (η %) are in good agreement with the results (η %) obtained by weight loss experiments.

3.3. UV-Visible Spectroscopy

UV-Visible spectroscopy provides a strong evidence for the interaction of the metal with the inhibitor. We obtained UV-Visible absorption spectra in the absence and presence of an optimum concentration of inhibitors (50 ppm) at 303 K before and after 6 h immersion of mild steel specimen as shown in Figure 9 (a, b).

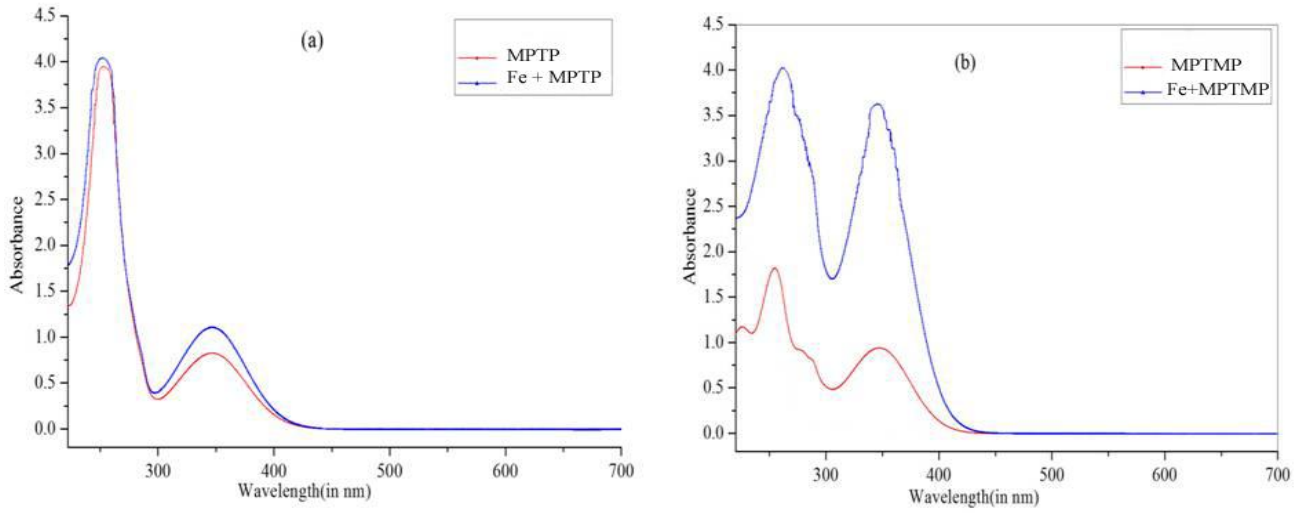

Figure 9. UV−visible spectra of a 15% HCl solution containing 50 ppm of inhibitor before and after 6 h of mild steel immersion (a) MPTP (b) MPTMP

The electronic absorption spectrum of both the inhibitors before the mild steel immersion shows bands in the UV-Visible region due to π-π* and n- π* transitions with a considerable charge transfer character. After 6 h immersion of mild steel in the presence of inhibitors, the observed change in the position and absorbance of the absorption maximum indicate interaction between the inhibitors and iron in solution. However, there was no significant change in the shape of the spectra. These experimental findings provide strong evidence for the complex formed between Fe^{2+} and inhibitors in a 15% HCl solution. UV-Visible observation confirms the formation of a protective film of metal-inhibitor complex on the metal surface.

3.4. Scanning electron microscopy

SEM photomicrographs for mild steel in a 15% HCl solution in the absence and presence of 50 ppm of MPTP and MPTMP are shown in Figure 10 (a-d).

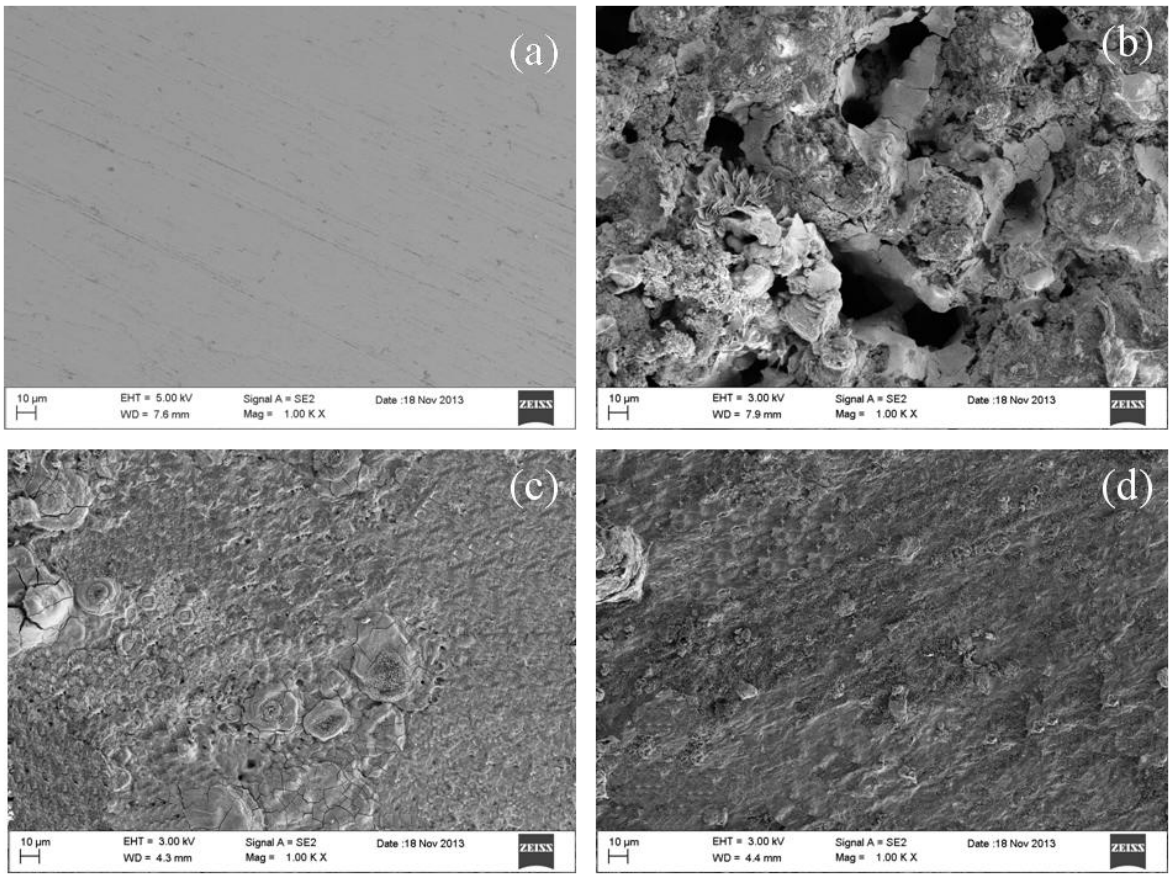

Figure 10. SEM image of mild steel in a 15% HCl solution after 6h immersion at 303 K (a) before immersion (polished) (b) After immersion without inhibitor (c) with inhibitor MPTP (d) with inhibitor MPTMP.

The morphology of the polished mild steel specimen (Fig. 10 a) is very smooth and shows no corrosion while mild steel specimens dipped in a 15% HCl solution in the absence of inhibitor (Fig. 10 b) is very rough and the surface is damaged due to metal dissolution. However, the presence of 50 ppm of inhibitor suppresses the rate of corrosion and surface damage has been diminished considerably (Figs. 10 c, d) as compared to the blank solution (Fig. 10 b) which suggests the formation of a protective inhibitor film at the mild steel surface.

3.5. Energy dispersive spectroscopy

The energy dispersive X-ray analysis (EDX) technique was employed in order to get information about the composition of the surface of the mild steel sample in the absence and presence of inhibitors in a 15% HCl solution. The results of EDX spectra are shown in Figure 11 (a, b, c and d).

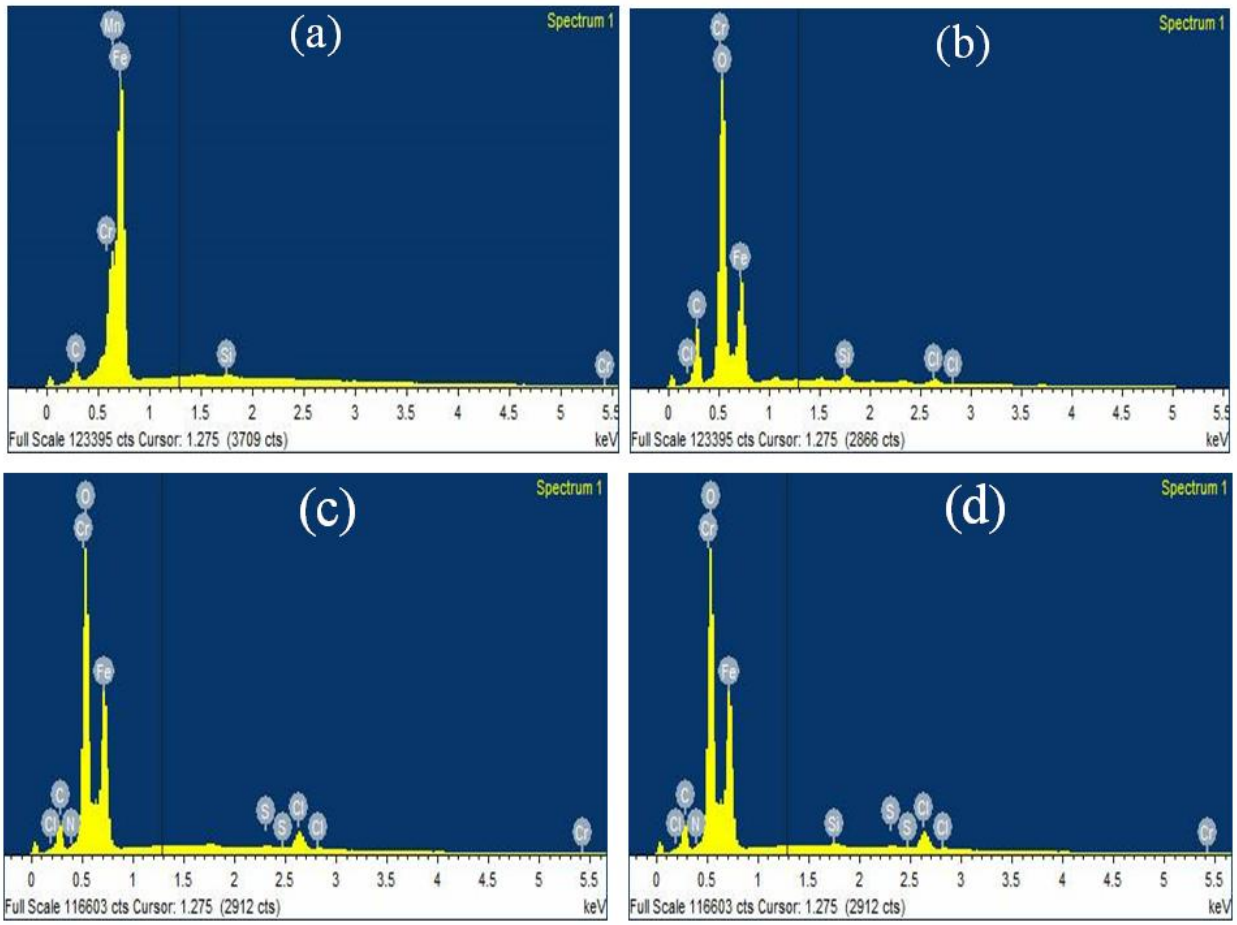

Figure 11. EDX spectra of mild steel specimens (a) polished (b) After immersion without inhibitor (c) with 50 ppm MPTP (d) with 50 ppm MPTMP.

The percentage atomic content of various elements of the polished, uninhibited and inhibited mild steel surface determined by EDX is shown in Table 6. The percentage atomic content of Fe for mild steel immersed in a 15% HCl solution is 83.12%, and those for mild steel dipped in an optimum concentration (50 ppm) of MPTP, and MPTMP are 71.16% and 69.84%, respectively. From Figure 11, the spectra of inhibited samples show that the Fe peaks are considerably suppressed, when compared with the polished and uninhibited mild steel samples. This suppression of Fe lines is due to the inhibitory film formed on the mild steel surface. The EDX spectra of inhibited mild steel contains the peaks corresponding to all the elements present in the inhibitor molecules indicating the adsorption of inhibitor molecules at the surface of mild steel.

Table 6. Percentage atomic contents of elements obtained from EDX spectra

Inhibitors	Fe	C	S	Cr	Mn	Cl	N	O
Polished mild Steel	85.26	12.46	-	0.86	0.46	-	-	-
Mild steel in blank HCl	83.12	15.68	-	0.67	0.28	2.29	-	6.36
Mild steel in MPTP	71.16	18.15	1.72	0.56	-	0.32	3.64	12.48
Mild steel in MPTMP	69.84	19.72	1.68	0.54	-	0.31	4.14	8.66

3.6. Atomic force microscopy

The three-dimensional AFM images of polished, uninhibited and inhibited mild steel samples are shown in Figure 12 a-d. The average roughness of the polished mild steel sample (Fig. 12 a) and mild steel sample in a 15% HCl solution without inhibitor (Fig. 12 b) were found to be 25 and 650 nm. It is clearly shown in Figure 12(b) that the mild steel sample is badly damaged due to the acid attack on the surface. However, in the presence of an optimum concentration (50 ppm) of MPTP and MPTMP as shown in Figure 12 (c, d), the average roughness were reduced to 82 and 65 nm, respectively. The lower value of roughness for MPTMP than MPTP reveals that MPTMP protects the mild steel surface more efficiently than MPTP in a 15% HCl solution.

3.7. Theoretical calculation

In order to study the effect of molecular structure on the inhibition efficiency, quantum chemical calculations were performed using the semi-empirical AM1 method and all the calculations were carried out with the help of complete geometry optimization. Optimized structures, E_{HOMO} and E_{LUMO} are shown in Figure13 (a, b). The quantum chemical parameters such as the energy of the highest occupied molecular orbital (E_{HOMO}), the energy of the lowest unoccupied molecular orbital (E_{LUMO}), energy gap (ΔE) and dipole moment (μ) were determined and summarized in Table 7. According to the frontier molecular orbital (FMO) theory of chemical reactivity, the formation of a transition state is due to interaction between HOMO and LUMO of reacting species. The smaller the orbital energy gap (ΔE) between the participating HOMO and LUMO, the stronger the interactions between two reacting species [35].

It was reported previously by some researchers that smaller values of ΔE and higher values of dipole moment (μ) are responsible for higher inhibition efficiency [36]. The lower values of the energy gap ΔE will render good inhibition efficiencies since the energy to remove an electron from the last occupied orbital will be minimized. According to HSAB theory hard acids prefer to co-ordinate to hard bases and soft acid to soft bases. Fe is considered as soft acid and will co-ordinate to molecule having maximum softness and small energy gap ($\Delta E = E_{LUMO} - E_{HOMO}$). From Table 7 it is clear that the highest value of E_{HOMO} (-8.8976 eV), μ (3.565 D) and lowest values of ΔE (7.7365 eV) and E_{LUMO} (-1.1611 eV) are found for MPTMP, indicating that MPTMP has more potency to get adsorbed on the mild steel surface resulting greater inhibition tendency than MPTP.

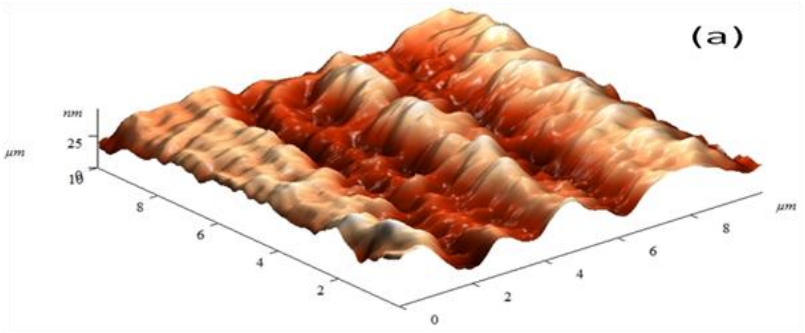

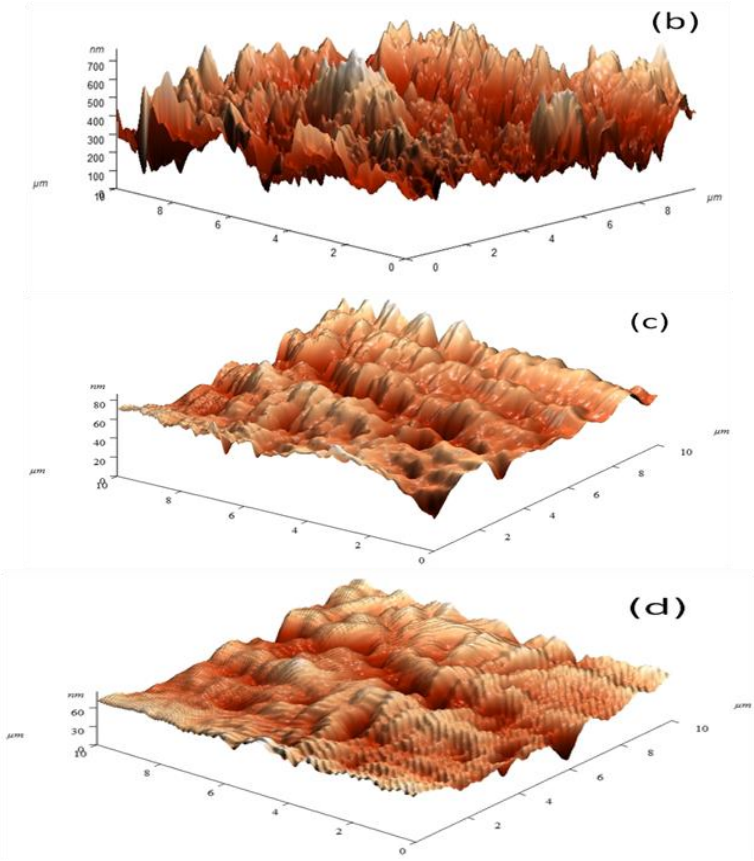

Figure 12. Atomic force micrographs of mild steel surface (a) polished mild steel, (b) mild steel in 15% HCl solution and (c) in presence of inhibitor MPTP (d) MPTMP.

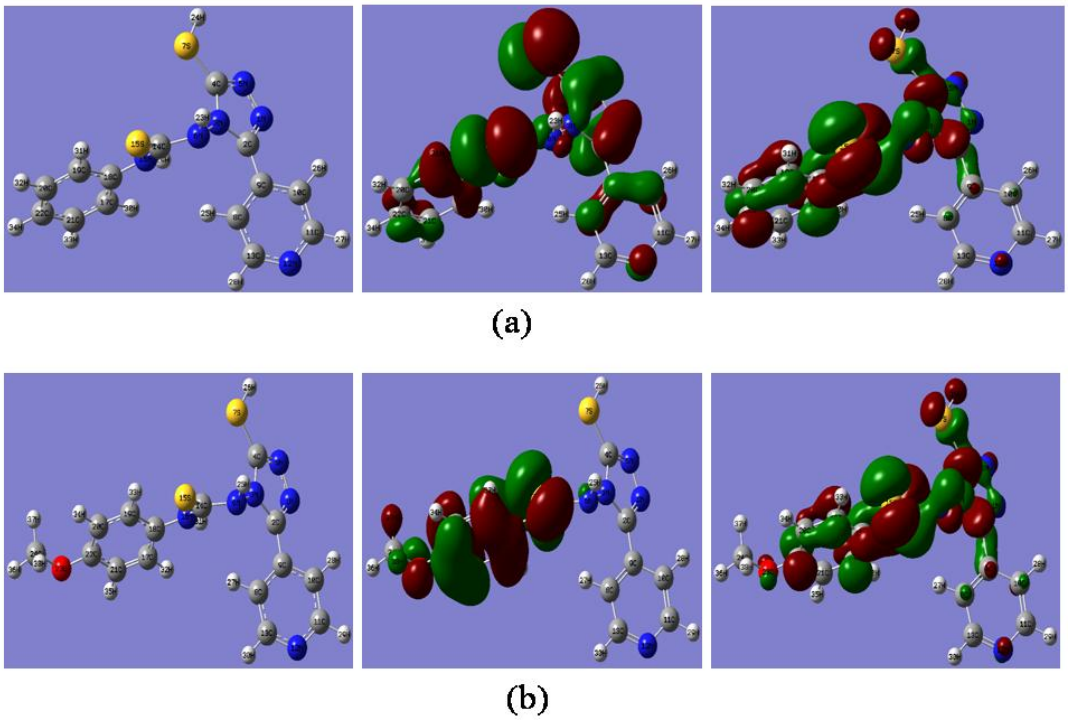

Figure 13. The optimized structure (left) and *HOMO* (center) and *LUMO* (right) distribution for molecules (a) MPTP, (b) MPTMP [H, Grey; C, Cyan; N, Blue; O, Red; S, Yellow].

Table 7. Quantum chemical parameters for different inhibitors

Inhibitor	$-E_{HOMO}$ (eV)	$-E_{LUMO}$ (eV)	ΔE (eV)	μ (D)
MPTP	9.1153	1.1156	7.999	2.938
MPTMP	8.8976	1.1611	7.7365	3.565

3.8. Mechanism of inhibition

Corrosion inhibition of mild steel in a 15% hydrochloric acid solution by both inhibitors (MPTP and MPTMP) can be explained on the basis of molecular adsorption. These compounds inhibit corrosion by controlling both anodic as well as cathodic reactions. In 15% hydrochloric acid solutions these inhibitors exist as protonated species. For both inhibitors the nitrogen atoms present in the molecules can be easily protonated in an acidic solution and convert into quaternary compounds. These protonated species adsorb onto the cathodic sites of the mild steel and decrease the evolution of hydrogen. The adsorption on the anodic site occurs through π-electrons of triazole, and phenyl rings and lone pair of electrons of nitrogen and sulfur atoms present in both the inhibitors which decrease the anodic dissolution of mild steel.

4. CONCLUSIONS

(1) The synthesized thiourea derivatives showed good inhibition efficiencies for the corrosion of mild steel in a 15% HCl solution and the inhibition efficiency increased with an increase in the concentration of inhibitor. The inhibiting performance of MPTMP is better than MPTP.

(2) Polarization studies showed that both tested inhibitors are a mixed type in nature.

(3) EIS measurements show that charge transfer resistance (R_{ct}) increases and double layer capacitance (C_{dl}) decreases in the presence of inhibitors which suggests the adsorption of the inhibitor molecules on the surface of mild steel.

(4) The results obtained from SEM, EDX, AFM and Langmuir adsorption isotherm suggest that the mechanism of corrosion inhibition is occurring mainly through the adsorption process.

(5) Quantum chemical results of MPTP and MPTMP showed a higher value of E_{HOMO}, a lower value of E_{LUMO}, and a smaller value of ΔE, indicating that both inhibitors are good at inhibiting corrosion of mild steel in a 15% HCl solution.

References

1. M.A. Migahed, A.M. Abdul-Raheim, A.M. Atta, W. Brostow, *Mater. Chem. Phys.* 195 (2010) 3590–3596.
2. D. Asefi, M. Arami, N.M. Mahmoodi, *Corros. Sci.* 52 (2010) 1801–1808.
3. G.N. Mu, X.H. Li, *J. Colloid Interface Sci*. 289 (2005) 184–192.
4. M.A. Amin, K.F. Khaled, Q. Mohsen, H.A. Arida, *Corros. Sci*. 52 (2010) 1684–1695.

5. E.M. Sherif, R.M. Erasmus, J.D. Comins, *Electrochim. Acta* 55 (2010) 3657–3663.
6. I.B. Obot, N.O. Obi-Egbedi, *Corros. Sci*. 52 (2010) 198–204.
7. P.B. Raja, M.G. Sethuraman, *Mater. Lett*. 62 (2008) 113–116.
8. F. Touhami, A. Aouniti, Y. Abed, B. Hammouti, S. Kertit, A. Ramdani, K. Elkacemi, *Corros. Sci*. 42 (2000) 929–940.
9. L. Tang, X. Li, L. Li, G. Mu, G. Liu, *Surf. Coat. Technol*. 201 (2006) 384–388.
10. M. Hosseini, S.F.L. Mertens, M. Ghorbani, M.R. Arshadi, *Mater. Chem. Phys*. 78 (2003) 800–808.
11. N.C. Subramanyam, B.S. Sheshardi, S.A. Mayanna, *Corros. Sci*. 34 (1993) 563–571.
12. S. D. Shetty, P. Shetty, H. V. S. Nayak, *J. Serb. Chem. Soc.* 71 (2006) 1073–1082.
13. B. M. Lawson, *Corrosion* 36 (1980) 493-97.
14. R. Agrawal, T. K. G. Namboodhiri, *Corros. Sci.* 30 (1990) 37-52.
15. I. Singh, *Corrosion* 49 (1993) 473-478.
16. S. M. Muralidharan, S. V. Iyer, *Anticorros. Methods Mater.* 44 (1997) 100-106.
17. F. B. Ravari, A. Dadgarinezhad, *Protection of Metals and Physical Chemistry of Surfaces*. 48 (2012) 265–269.
18. A. M. Al-Sabagh, M. A. Migahed, M. Abd El-Raouf, *Chem. Eng. Commun.* 199 (2012) 737-750.
19. M. Yadav, D. Behera, U. Sharma, *Corros. Eng. Sci. Technol.* 48 (2013) 19-27.
20. M. Yadav, D. Behera, U. Sharma, *Arab. J. Chem.* DOI: 10.1016/j.arabjc.2012.03.011.
21. M. Yadav, U. Sharma, *J. Mater. Environ. Sci.* 2 (2011) 407-414.
22. R. El-Sayed, *Indian J. Chem.* 45*B* (2006) 738-746.
23. ASTM, G 31–72, American Society for Testing and Materials, Philadelphia, PA, 1990.
24. M.J.S. Dewar, E.G. Zoebisch, E.F. Healy, J.J.P. Stewart, *J. Am. Chem. Soc.* 107 **(**1985) 3902-3909.
25. S.S. Abdel-Rehim, M.A.M. Ibrahim, K.F. Khaled, *J. Appl. Electrochem*. 29 (1999) 593-599.
26. L. Fragoza-Mar, O. Olivares-Xometl, M.A. Domínguez-Aguilar, E.A. Flores, P. Arellanes-Lozada, F. Jimenez-Cruz, *Corros. Sci*., 61 (2012) 171–184.
27. I. Dehri, M. Ozcan, *Mater. Chem. Phys*. 98 (2006) 316-323.
28. X. Wang, H.; Yang, F. Wang, *Corros. Sci.* 53 (2011) 113–121.
29. M. Behpour, S.M. Ghoreishi, N. Soltani, M. Salavati-Niasari, M. Hamadanian, A.Gandomi, *Corros. Sci*. 50 (2008) 2172-2181.
30. M.S. Morad, A.M. Kamal El-Dean, *Corros. Sci*. 48 (2006) 3398-3412.
31. G.N. Mu, X.H. Li, Q. Qu, J. Zhou, *Corros. Sci*. 48 (2006) 445-459.
32. M. Lebrini, M. Lagrene´e, H. Vezin, M. Traisnel, F. Bentiss, *Corros. Sci*. 49 (2007) 2254-2269.
33. H. Gerengi, H.I. Sahin, *Ind. Eng. Chem. Res.* 51 (2012) 780-787.
34. M. Lebrini, F. Robert, A. Lecante, C. Roos, *Corros. Sci.* 53 (2011) 687–695.
35. S. Xia, M. Qiu, L. Yu, F. Liu, H. Zhao, *Corros. Sci*. 50 (2008) 2021-2029.
36. V.S. Sastri, J.R. Perumareddi, *Corrosion* 53 (1997) 617-622.